Journal of
Composites Science

MDPI

Article

Evaluation of the Self-Healing Behaviour of Structural Polyamide 6 (PA6)/Poly(butylene-adipate-terephthalate) (PBAT) Blends

Laura Simonini [1,2,*], Giuseppe Fuoli [1,2], Alessandro Sorze [1,2], Alessandro Pegoretti [1,2] and Andrea Dorigato [1,2]

[1] Department of Industrial Engineering, University of Trento, Via Sommarive 9, 38121 Trento, Italy; alessandro.sorze@unitn.it (A.S.); alessandro.pegoretti@unitn.it (A.P.); andrea.dorigato@unitn.it (A.D.)
[2] National Interuniversity Consortium of Materials Science and Technology (INSTM), Via Giusti 9, 50121 Florence, Italy
* Correspondence: laura.simonini@unitn.it

Abstract

In this study, polyamide 6/poly(butylene-adipate-terephthalate) (PA6/PBAT) blends, potentially applied as novel self-healing matrices for structural composites, were developed and characterized. The blends were melt-compounded at different PBAT amounts (from 20 up to 50%vol) and hot pressed. Rheological analysis showed a decreased in the storage and loss moduli of PA6 with PBAT, maintaining viscosity levels suitable for conventional melt-processing operations. FT-IR and FESEM observations demonstrated the formation of blends with immiscible morphology and uniformly dispersed PBAT domains. Quasi-static tensile tests showed a progressive decrease in tensile modulus and strength with PBAT, but a strong improvement in the elongation at break. The blend containing 30%vol PBAT showed satisfactory stiffness (2.2 GPa), strength (42 MPa) and elongation at break (10.5%) compared to PA6 (3.4 GPa, 62 MPa and 5.2%), thus this formulation was selected for self-healing assessment. Its repair efficiency was quantified as recovery of the fracture toughness (K_{IC}) after a thermal treatment at 150 °C for 30–120 min under pressure from 1–3 MPa. The highest healing efficiency (28%) was obtained after 120 min under 1 MPa, conditions at which the PBAT reduced its viscosity and flowed across the crack interface. Therefore, the blend with 30%vol PBAT will be considered in future for the preparation of multifunctional composites with thermal self-healing capability.

Keywords: PA6; PBAT; blends; fracture toughness; self-healing

1. Introduction

Thermoplastic polymer matrix composites (PCMs) are widely used in transportation [1], aerospace [2], construction [3] and energy sectors [4], since they are characterized by high strength-to-weight ratio, corrosion resistance and design versatility. The market of thermoplastic PCMs has been globally valued equal to $32.2 billion in 2021. Its growth is associated to a compound annual growth rate (CAGR) equal to 7.8%, thus it will reach $62.6 billion by 2030 [5]. However, thermoplastic PCMs suffer from microdamage during service, such as cracks and voids in the matrix [6,7], fiber/matrix interfacial debonding [8–14] or interlaminar fracture [15,16]. These types of damages cause a progressive deterioration of the mechanical integrity and reliability of PCMs. Moreover, the repair and maintenance operations of in service PCMs are often complex and costly. In this scenario, there is a significant interest in the development of thermoplastic PCMs with self-healing capabilities, as a strategy to increase their reliability, reduce maintenance and extend service lifetime [17]. Self-healing composites are able to recover their structural integrity

Academic Editor: Roberto Scaffaro

Received: 8 July 2026
Revised: 7 August 2026
Accepted: 10 August 2026
Published: 18 August 2026

after damage by partially mimicking the biological self-repair mechanisms observed in nature [18]. They can be found as extrinsic and intrinsic systems. The extrinsic systems are based on healing agents encapsulated in microcapsules [19] or vascular networks [20], which are released upon fracture to fill and repair the damaged area. However, they become inactive once the healing agent has been used, enabling only one repair event. Moreover, microcapsules and networks may act as stress concentrators causing defects in the matrix or they can increase the matrix viscosity, making processing more difficult [21]. Conversely, intrinsic systems are based on reversible molecular interactions within the matrix, such as hydrogen bonds, supramolecular associations or thermally activated chain mobility [22–25] to heal the cracks. The advantage of these systems is that they can heal repeatedly upon external stimuli (such as heat, light, electrical and/or magnetic field) under mild conditions, making them highly attractive for high-performance thermoplastics. Recently, intrinsic self-healing through the incorporation of a thermoplastic polymer into the matrix is finding increasing attraction. The thermoplastic polymer is physically blended into the matrix (either thermoplastic or thermosetting) and acts as the self-healing agent by melting (or softening) and flowing into damaged area to be healed. For instance, Savioli et al. [26] blended poly(lactic acid) (PLA) with poly(butylene adipate-co-terephthalate) (PBAT) from 10 to 30% by weight, obtaining blends with immiscible morphology constituted by PBAT domains dispersed within the PLA matrix. The addition of PBAT reduced the PLA brittleness and imparted self-healing ability, restoring up to 64% of the original fracture toughness upon thermal mending at 140 °C. Peñas-Caballero et al. [27] investigated an epoxy resin blended with poly(ethylene-co-methacrylic acid) (EMAA), resulting in immiscible thermoplastic domains within the thermosetting matrix, achieving up to 45% recovery of tensile strength upon thermal mending at 150 °C.

In particular, polyamide 6 (PA6) has received in recent years increasing attention for use in the fabrication of thermoplastic PCMs for high-performance structural applications [28]. PA6 is a thermoplastic polymer that is synthesized through the ring-opening polymerization of caprolactam [29]. Despite its high stiffness (2.5–3.3 GPa) and strength (70–85 MPa) [30], it can exhibit limited resistance to crack initiation and propagation under mechanical loading, which may compromise the durability of structural components [31]. For this reason, blending PA6 with a thermoplastic polymer that can simultaneously act both as a toughening and self-healing agent may be a suitable solution [32]. In this context, Perin et al. [33] developed blends of PA6 with a cyclic olefin copolymer (COC) as healing agent. Initially, they studied PA6/COC blends compatibilized with ethylene glycidyl methacrylate (E-GMA) showing that, upon thermal activation, COC flowed and filled the PA6 microcracks, thus enabling a partial restoration of its original fracture toughness (68% under impact conditions). Subsequently [34], they adjusted the E-GMA content and healing temperature in PA6/COC blends, finding that a higher compatibilizer amount (i.e., 5%wt) improved the interfacial adhesion and the self-healing efficiency of the blends. However, in all these systems the inherent brittleness of COC limited the fracture toughness of PA6. Poly(butylene adipate terephthalate) (PBAT) is a biodegradable copolyester of adipic acid, 1,4-butanediol and terephthalic acid. It is widely considered as a fully biodegradable alternative to low-density polyethylene (LDPE), having many similar properties, including flexibility and resilience, making it suitable for the production of plastic bags and wraps [35]. It has relatively low melting point (115–120 °C), which can promote an intrinsic self-healing mechanism, since it can melt and flow into cracks when heated to moderate temperatures (i.e., 120–150 °C). Therefore, the combination of the thermo-mechanical performance of PA6 with the ductility of PBAT creates opportunities for designing novel self-healing thermoplastic matrices for structural applications. To the best of the authors' knowledge, there are

no reported studies focused on the investigation of the thermo-mechanical and self-healing properties of these blends.

Therefore, in this paper novel thermoplastic self-healing polymer blends of PA6 containing 20, 30, 40 and 50%vol of PBAT were developed and characterized. The PA6 acted as the structural matrix and PBAT as the thermoplastic self-healing agent. The objective of this research was to identify the most promising blend composition to combine satisfactory structural performance and self-healing capability. In order to achieve this goal, the obtained compositions were characterized in terms of their rheological, morphological, and thermo-mechanical properties, with particular attention to their fracture toughness both under quasi-static and impact conditions. The self-healing capability was evaluated by measuring the recovery of fracture toughness after a thermal healing treatment performed at 150 °C at different times (from 30 to 120 min) and applied pressures (from 1 to 3 MPa). These materials could be then utilized in the future as self-healing matrices in multifunctional composite laminates, in combination with glass and carbon fibers.

2. Materials and Methods

2.1. Materials

The matrix material used in this study was a commercial polyamide 6 (PA6, Radilon® S BF 990 GY, Radici Group, Bergamo, Italy), supplied as pellets. According to the manufacturer's specifications, the material has a density of 1.14 g/cm^3, an average molecular weight (M_w) of approximately 60,000 g/mol, a melt flow index (MFI) of 20 g/10 min (275 °C, 5 kg), and a melting temperature of about 220 °C. The healing phase consisted of a commercial poly(butylene adipate terephthalate) (PBAT, Technipol® Bio 1160, Sipol S.p.A., Mortara, Italy), supplied as approximately 3 mm pellets. The PBAT has a density of 1.23 g/cm^3, an average molecular weight of about 50,000 g/mol, an MFI of 20 g/10 min (160 °C, 2.16 kg), and a melting temperature of approximately 115 °C, as reported by the manufacturer. Preliminary trials were also performed using a commercial compatibilizing agent to improve the interfacial adhesion between PA6 and PBAT, i.e., an epoxy-functional chain extender Joncryl® ADR 4468 (J), supplied by BASF GmbH (Ludwigshafen am Rhein, Germany). This compatibilizer was selected based on the author's previous studies [26]. However, the compatibilizer did not provide a satisfactory improvement in the mechanical properties or self-healing performance (see Supplementary Materials). Consequently, the present study focused on uncompatibilized PA6/PBAT blends.

2.2. Sample Preparation

Prior to processing, PA6 and PBAT pellets were dried in a ventilated oven at 50 °C for 48 h to remove residual moisture. The desired blend compositions were prepared by manually premixing the components prior to being simultaneously introduced in an internal mixer (Thermo Haake Rheomix 600, Thermo Fisher Scientific, Waltham, MA, USA) equipped with counter-rotating rotors. Melt compounding was carried out at 230 °C for 5 min at a rotor speed of 60 rpm. The compounded materials were subsequently grinded in a Piovan® RN166/1 granulator (Piovan SpA, Venice, Italy) to produce pellets smaller than 2 mm, then compression molded using a laboratory hot press (Carver Inc., Wabash, IN, USA) maintained at 220 °C. The material was first allowed to melt for 3.5 min without applied pressure and was then consolidated under a pressure of 3.4 MPa for additional 4 min. The molded plates were cooled to room temperature using a circulating water system at approximately 10 °C/min. After this procedure, square plates with dimensions of 120 × 120 × 2 mm^3 were produced. To prepare specimens for fracture toughness testing, plates with a thickness of 5 mm were manufactured using the same molding conditions, except that the initial melting stage was extended to 6 min to ensure complete melting

throughout the increased thickness before pressure was applied. A schematic representation of the sample preparation process is shown in Figure 1, while the list of the compositions is summarized in Table 1.

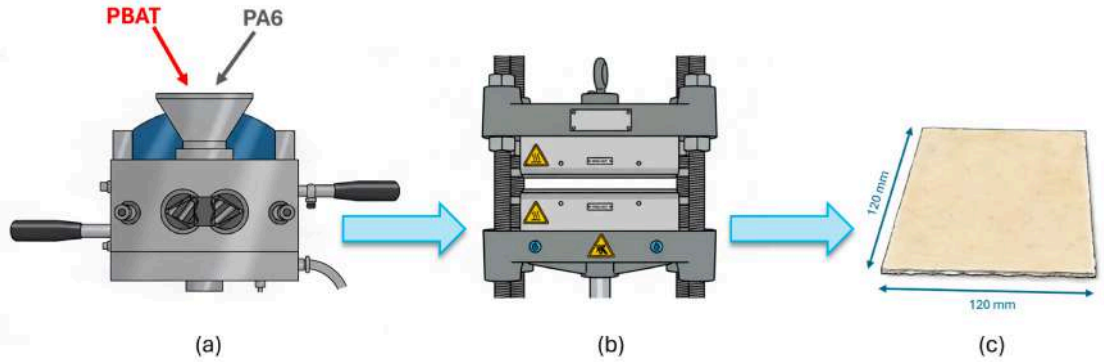

Figure 1. Schematic representation of sample preparation: (**a**) melt compounding of dried PA6 and PBAT pellets, (**b**) compression molding of the ground compounded blend, and (**c**) final square plates with dimensions of 120 × 120 × 2 or 120 × 120 × 5 mm^3.

Table 1. List of the prepared blends with their relative composition.

Samples	PA6 (%vol)	PBAT (%vol)	PA6 (%wt)	PBAT (%wt)
PA6	100	-	100	-
PA6-20PBAT	80	20	79	21
PA6-30PBAT	70	30	68	32
PA6-40PBAT	60	40	58	42
PA6-50PBAT	50	50	48	52
PBAT	-	100	-	100

2.3. Experimental Techniques

2.3.1. Rheological Properties

The viscoelastic behaviour of the blends was investigated using a Discovery Hybrid Rheometer (DHR-2, TA Instruments, New Castle, DE, USA) operating in parallel-plate configuration (25 mm diameter, 1 mm gap). Frequency sweep tests were performed at 230 °C using a strain amplitude of 1% over an angular frequency range of 0.1–100 rad/s. The storage modulus (G′), loss modulus (G″), and complex viscosity (η*) were determined for each composition. One specimen was tested per formulation.

2.3.2. Chemical and Microstructural Properties

The chemical structure of the blends was examined by Fourier-transform infrared spectroscopy (FT-IR) in attenuated total reflectance (ATR) mode using a Spectrum One spectrometer (PerkinElmer, Shelton, CT, USA). Spectra were collected over the 4000–650 cm^{-1} wavenumber range with a resolution of 4 cm^{-1} by averaging four scans. One specimen was analyzed for each composition.

The morphology of both virgin and healed blends was investigated on cryo-fractured surfaces using a field-emission scanning electron microscope (FESEM, Zeiss Supra 40, Carl Zeiss AG, Oberkochen, Germany) operated at an accelerating voltage of 3.5 kV. Prior to imaging, the specimens were sputter-coated with an approximately 5 nm thick Pt/Pd (80:20) conductive layer. The average diameter of the dispersed PBAT domains was measured from the micrographs using ImageJ® software (version 1.53a).

2.3.3. Thermal Properties

Thermal properties were evaluated by differential scanning calorimetry (DSC) using a Mettler DSC30 calorimeter (Mettler Toledo, Columbus, OH, USA) under a nitrogen atmosphere (100 mL/min). Samples were subjected to a first heating scan, a cooling scan and a second heating scan between −80 °C and 250 °C at a heating/cooling rate of 10 °C/min. The glass transition temperature (T_g), melting temperature (T_m) and melting enthalpy (ΔH_m) of both PA6 and PBAT were determined. Equation (1) was used to calculate the degree of crystallinity of PA6 (or PBAT) phases (X) in the blends,

$$X(\%) = \frac{\Delta H_m}{\Delta H_m^0 \times w} \times 100 \quad (1)$$

where ΔH_m is the measured melting enthalpy of PA6 (or PBAT) and $\Delta H_m{}^0$ is the melting enthalpy of the 100% crystalline PA6 (230.0 J/g [36]) or 100% crystalline PBAT (114.0 J/g [26]), while w is the weight fraction of PA6 (or PBAT) in the blends. One specimen was tested for each composition.

2.3.4. Mechanical Properties

Quasi-static tensile tests were carried out on an Instron 5969 universal testing machine (Instron Inc., Norwood, MA, USA) equipped with a 10 kN load cell using ISO 527-4 (Plastics—Determination of tensile properties—International Organization for Standardization: Geneva, Switzerland, 2023) type 1BA specimens. The elastic modulus was determined at a crosshead speed of 0.25 mm/min up to 1% strain using an extensometer (Instron 2620-601, gauge length 12.5 mm), and calculated as the secant modulus between 0.05% and 0.25% strain according to ISO 527-4. Tensile strength and elongation at break were measured at a crosshead speed of 10 mm/min without the extensometer. At least five specimens were tested for each composition. Regarding the modelling of the mechanical properties of the prepared blends (i.e., elastic modulus, stress and strain at break), the Maxwell–Eucken (ME) model was used. The ME model is able to predict the mechanical properties of a blend characterized by a droplet-matrix morphology, with the expression reported in Equation (2) [37],

$$P_b = \frac{P_{PA6}v + P_{PBAT}(1-v)\frac{3P_{PA6}}{2P_{Pa6}+P_{PBAT}}}{v + (1-v)\frac{3P_{PA6}}{2P_{PA6}+P_{PBAT}}} \quad (2)$$

where P_b is the property of the blend, v is the volume fraction of PA6 in the sample, P_{PA6} is the property of neat PA6, and P_{PBAT} is the property of neat PBAT.

The Vicat softening temperature (VST) was measured according to ASTM D1525 (Standard Test Method for Vicat Softening Temperature of Plastics. ASTM International: West Conshohocken, PA, USA, 2017) using an MP/3 HDT-Vicat apparatus (ATS Faar Industries, Milan, Italy) at a heating rate of 120 °C/h under a 50 N load. Three specimens were tested for each composition.

Fracture toughness was evaluated on Single Edge Notched Bending (SENB) specimens following ASTM D5045 (Standard Test Methods for Plane-Strain Fracture Toughness and Strain Energy Release Rate of Plastic Materials. ASTM International: West Conshohocken, PA, USA, 2014). The tests were carried out on Single Edge Notched Bending (SENB) specimens, having nominal dimensions of 44 × 10 × 5 mm^3, an initial notch length of 5 mm and a span length of 40 mm. Quasi-static tests were performed in three-point bending using the Instron 5969 machine at a crosshead speed of 10 mm/min, while impact tests were carried out according to ISO 17281 (Plastics—Determination of fracture toughness (GIC and KIC) at moderately high loading rates (1 m/s). International Organization for Standardization: Geneva, Switzerland, 2002) using a CEAST Charpy impact tester (Darmstadt, Germany)

equipped with an instrumented hammer (0.834 kg striker, impact speed 1 m/s). At least six specimens were tested for each condition. From the load-displacement curves deriving from both quasi-static and impact tests it was possible to determine the maximum load sustained by the samples (P_{max}), while the critical stress intensity factor (K_{IC}) was calculated according to Equation (3),

$$K_{IC} = \frac{P_{max}}{B\sqrt{W}} \cdot f(x) \quad (3)$$

where B and W are respectively the thickness and the width of the specimen and f(x) is a value provided in the standard as function of (x = a/W), where a is the notch length. Furthermore, in accordance with ASTM D5045 standard, the critical strain energy release rate (G_{IC}) values in quasi-static mode were obtained by integrating the load-displacement curves and evaluating the system compliance, according to the expression reported in Equation (4),

$$G_{IC} = \frac{\Delta U}{BW\varphi} \quad (4)$$

where ΔU is the difference of the total energy absorbed by the sample and the energy absorbed in the indentation tests, and φ is a value reported in the standard as function of x = a/W.

2.3.5. Evaluation of the Self-Healing Efficiency

After fracture testing, the two halves of each SENB specimen were repositioned inside an iron vice (Figure 2a) equipped with a 3D-printed alignment holder to ensure that they were perfectly aligned. Then, they were subjected to contact pressures of 1, 2 or 3 MPa adjusted though a calibrated torque wrench. Subsequently, they were thermally treated in an oven at 150 °C for 30, 60 or 120 min. The healing temperature was selected based on preliminary rheological measurements of PBAT (Figure 2b). The viscosity as a function of temperature was measured using the same rheometer in parallel-plate configuration (25 mm diameter) at a constant angular frequency of 100 rad/s. A pronounced viscosity decrease was observed around 140 °C, indicating the onset of sufficient chain mobility. Therefore, a healing temperature of 150 °C was selected to promote PBAT melting, flow and interdiffusion across the crack interface while avoiding thermal degradation.

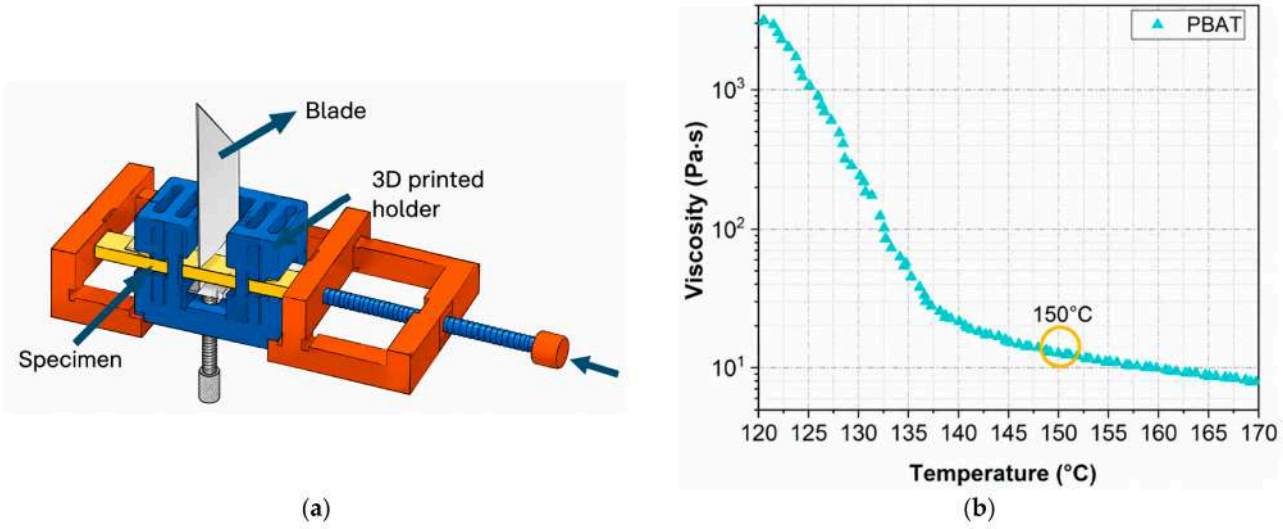

Figure 2. (**a**) Schematic representation of the lab-made device used for the thermal healing process and, (**b**) evolution of the viscosity of PBAT as a function of temperature.

The healed SENB specimens were retested under impact loading to determine the fracture toughness of the healed material ($K_{IC,H}$). The healing efficiency (HE) was then

quantified as the ratio between the fracture toughness of the healed and virgin specimens, according to Equation (5).

$$\mathrm{HE} = \frac{K_{IC,H}}{K_{IC}} \quad (5)$$

2.3.6. Statistical Analysis

Data have been presented as mean ± standard deviation. Statistical differences among groups were evaluated by one-way analysis of variance (ANOVA), followed by Tukey's honestly significant difference (HSD) post-hoc test, using a significance level of $\alpha = 0.05$.

3. Results

3.1. Rheological Measurements

The results obtained from the dynamic rheological measurements on the prepared blends are reported in Figure 3a–c. Specifically, the storage modulus (G′), loss modulus (G″) and complex viscosity (η*) as a function of angular frequency are shown.

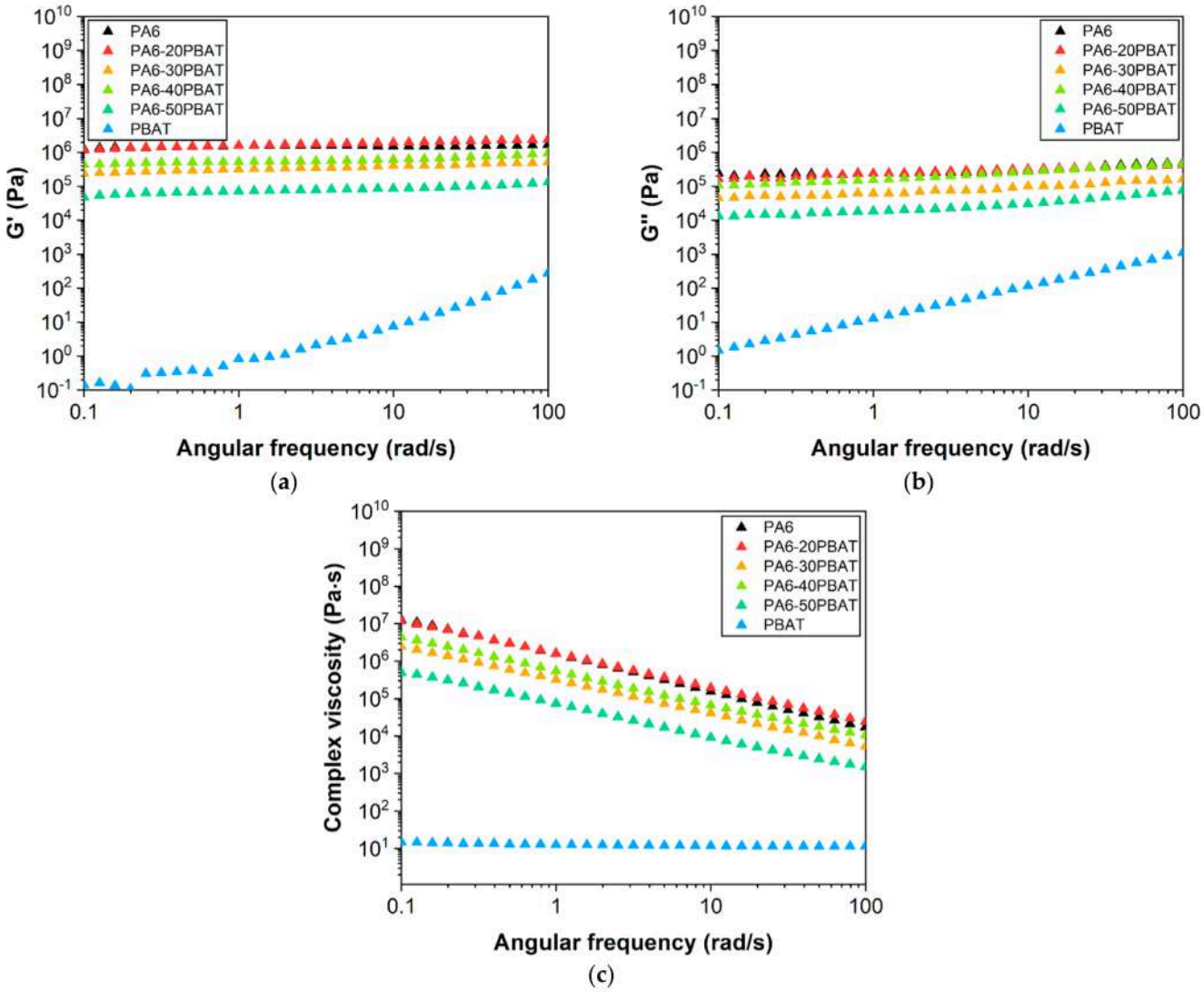

Figure 3. Dynamic rheological behaviour of the produced blends (T = 230 °C). Trends of (**a**) storage modulus, (**b**) loss modulus and (**c**) complex viscosity as a function of the angular frequency.

Neat PA6 exhibits the highest G′ over the entire frequency range. The incorporation of PBAT leads to a general decrease in G′, indicating a reduction in blend stiffness and

elastic response, as PBAT acts as a tougher dispersed phase within the PA6 matrix. Also Yildirim et al. [38] observed a similar decrease when they blended PA6 with a thermoplastic elastomer (TPE), that acted as a tougher phase in the blend. On the other hand, PA6 exhibits the highest G″ over the entire frequency range. As PBAT content increases, G″ decreases progressively, following the same trend observed for G′. However, G′ is always higher than G″ for PA6 and all the relative blends, indicating a predominantly elastic (solid-like) behaviour over a liquid-like one. In contrast, PBAT exhibits G″ > G′, indicating a predominantly viscous liquid-like response. The absence of a crossover point (G′ = G″) in the explored frequency range further confirms that the relaxation times of these systems are relatively long, and the elastic network is maintained even at low frequencies. The complex viscosity (η*) decreases with increasing angular frequency for all compositions, demonstrating a clear shear-thinning (pseudoplastic) behaviour. Neat PA6 shows the highest viscosity (of the order of 107 Pa·s), while PBAT exhibits the lowest one (about 101 Pa·s). The blends display intermediate values, decreasing progressively with the PBAT amount. This indicates that PBAT lowers the viscosity of the system, improving its processability by melt compounding. In particular, the PA6-50PBAT blend exhibits the largest decrease in G′, G″ and complex viscosity compared with the other formulations, progressively approaching those of neat PBAT. This trend suggests that the viscoelastic response becomes increasingly dominated by the PBAT phase, supporting the hypothesis of a transition to a morphology characterized by phase continuity. Overall, the melt viscosity values of all the investigated blends remain within a suitable range to ensure efficient processability under standard melt-processing conditions.

3.2. Chemical and Microstructural Characterization

In Figure 4, the FT-IR spectra of the neat matrices and of the prepared blends are shown.

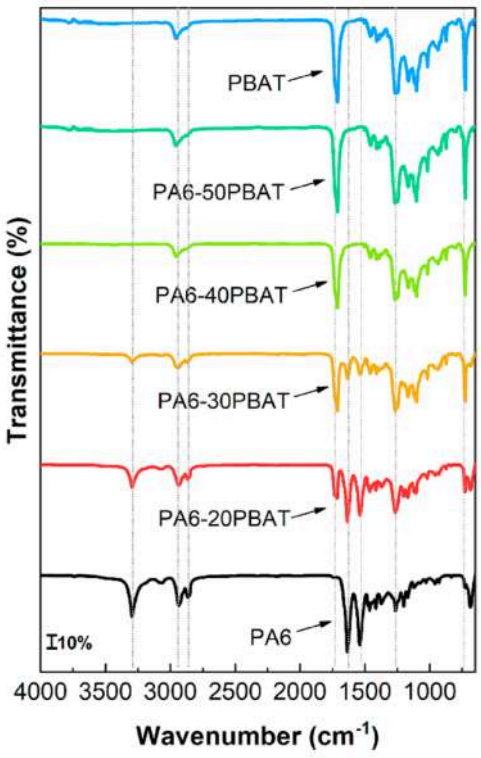

Figure 4. FT-IR spectra of neat PA6, neat PBAT and of the prepared blends.

Neat PA6 exhibits a characteristic N–H stretching vibration at 3292 cm^{-1}, along with the asymmetric and symmetric stretching vibrations of the –CH_2– groups at 2934 and 2853 cm^{-1},

respectively [39]. In addition, the absorption bands at 1637 cm^{-1} and 1535 cm^{-1} are assigned to the C=O stretching vibration of amide I and to the combined N–H bending and C–N stretching vibration of amide II, respectively [40]. The peak at 1263 cm^{-1} corresponds to amide III, associated with coupled C–N stretching and N–H bending modes [41]. In contrast, PBAT is characterized by the CH_2 asymmetric stretching band at 2956 cm^{-1}, the strong ester carbonyl (C=O) absorption at 1711 cm^{-1}, the aromatic C=C stretching vibration at 1507 cm^{-1}, and the bands at 1268, 1124, 1099 and 929 cm^{-1}, which are associated with C–O stretching vibrations of the polyester backbone [42,43]. The FTIR spectra of the PA6/PBAT blends display no additional bands beyond those of neat PA6 and PBAT, nor do they show significant peak shifts. This suggests the absence of strong specific interactions or chemical reactions between the two polymers, supporting the hypothesis that the PA6/PBAT system is immiscible. Furthermore, the characteristic peaks of PA6 progressively decrease in intensity with the PBAT content, while the PBAT bands become more pronounced and visible, reflecting the higher concentration of the PBAT phase in the blends.

Figure 5a–f show the FESEM micrographs of the cryo-fractured surfaces of the prepared formulations. For each formulation, the average and standard deviation of the PBAT domains (D) within the PA6 matrix is reported.

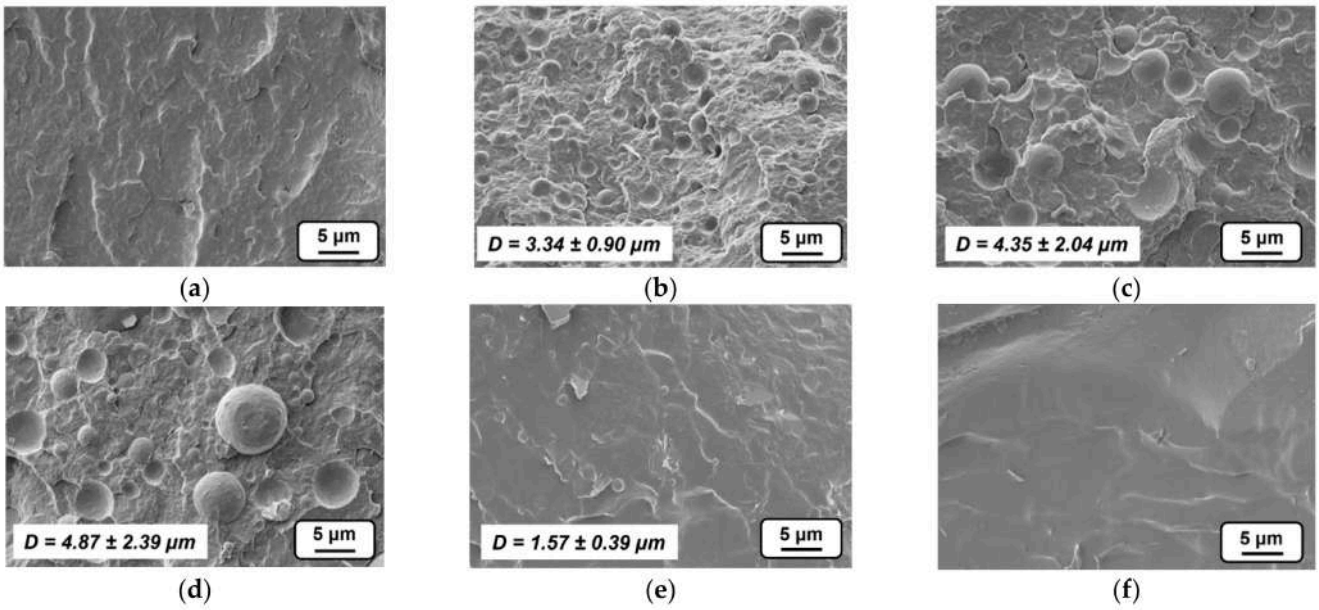

Figure 5. FESEM micrographs of the neat polymers and of the relative blends. (**a**) PA6, (**b**) PA6-20PBAT, (**c**) PA6-30PBAT, (**d**) PA6-40PBAT, (**e**) PA6-50PBAT and (**f**) PBAT. The average size of PBAT domains (D) is reported for each blend.

Neat PA6 (Figure 5a) shows a relatively smooth fracture surface, whereas PBAT shows a more ductile fracture morphology (Figure 5f), which is consistent with its intrinsically higher ductility. Figure 5b–d display the typical morphology of immiscible polymer blends, in which PBAT forms spherical domains dispersed within the continuous PA6 matrix. These domains have rather good adhesion to the PA6 matrix, with no significant interfacial debonding or void formation. As the PBAT content increases from 20 to 40%vol, a progressive increase in domain size is observed. The PA6–20PBAT blend shows small domains with an average size of 3.34 ± 0.90 µm. By increasing the PBAT content to 30 and 40%vol a marked increase in average domain size is detected, reaching 4.35 ± 2.04 µm and 4.87 ± 2.39 µm, respectively. This increase highlights the reduced ability of the PA6 matrix to stabilize the dispersed phase as the concentration of PBAT increases, resulting in less homogeneous morphologies. A similar behaviour was observed in previous works by our group, in which

PA6/cyclic olefin copolymer (COC) blends exhibited a droplet-like morphology, with the COC domain increasing in size as the weight content increased [44]. Moreover, the reduced ability of the PA6 matrix to stabilize the dispersed phase and the coalescence tendency of the PBAT domains at elevated concentrations are supported by the higher standard deviations observed for the PA6–30PBAT and PA6–40PBAT blends (i.e., 2.04 μm and 2.39 μm, respectively). Interestingly, the PA6–50PBAT blend (Figure 5e) exhibits smaller (1.57 ± 0.39 μm) and fewer domains, possibly suggesting that a phase inversion occurred at this composition (the results of rheology in Section 3.1 and of mechanical properties in Section 3.4 support this hypothesis).

3.3. Thermal Characterization

Figure 6a–c show the DSC thermograms of the prepared blends, while the most important results are summarized in Table 2.

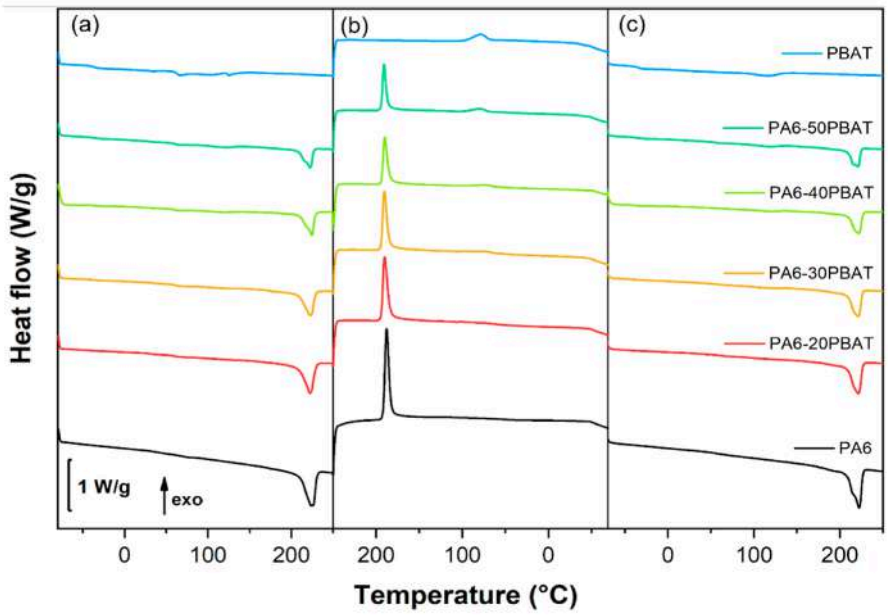

Figure 6. DSC thermograms of the produced blends: (**a**) first heating, (**b**) cooling and (**c**) second heating scans.

In the first heating scan, neat PA6 exhibits a melting temperature (T_m) of 224.9 °C and a degree of crystallinity of 30%, whereas a weak glass transition temperature (T_g) signal is detected at approximately 60 °C. Similar values can be found in literature on the same PA6 matrix [29]. In contrast, PBAT shows a T_m of 117.1 °C and a degree of crystallinity of approximately 9%. Also in this case, the glass transition temperature (T_g) is observed as a weak signal at approximately −38 °C. These values are in agreement with those reported in literature [26]. The progressive incorporation of PBAT does not induce significant variations in the T_g and T_m of PA6, further supporting the immiscibility of the PA6/PBAT system. Nevertheless, the addition of PBAT slightly increases the crystallinity of the PA6 phase, which passes from 30.0% for neat PA6 to 38.1% at a PBAT content of 40%vol. This progressive increase may be attributed to the presence of dispersed PBAT domains, which favors the crystallization of PA6 by acting as preferential nucleation sites. A similar observation was reported by Xiao et al. [45] for PLA/PBAT blends, where PBAT addition markedly increased PLA crystallinity since it promoted the nucleation of crystals. In the second heating scan, the melting temperatures of neat polymers and blends remain comparable to those observed in the first scan. The crystallinity values are overall similar to those measured during first heating stage, suggesting that the materials exhibit stable

crystallization behaviour and that melting and crystallization do not induce significant changes in crystalline content [29]. Overall, DSC results indicate that the incorporation of PBAT does not significantly alter the main thermal transitions of the PA6 matrix, confirming the immiscible nature of the prepared blends and suggesting limited interaction between the two polymer phases. A similar behaviour has previously observed by our group for PA6/COC and PA6/polycaprolactone (PCL) blends [29].

Table 2. Results of the DSC tests on neat PA6, neat PBAT and on the prepared blends.

Samples	$T_{m,PA6}$ (°C)	$T_{m,\ PBAT}$ (°C)	$\Delta H_{m,PA6}$ (J/g)	$\Delta H_{m,PBAT}$ (J/g)	X_{PA6} (%)	X_{PBAT} (%)
First heating						
PA6	224.9	-	69.1	-	30.0	-
PA6-20PBAT	222.5	-	61.7	-	34.0	-
PA6-30PBAT	223.0	-	50.3	-	32.2	-
PA6-40PBAT	224.4	119.5	37.5	2.3	38.1	4.8
PA6-50PBAT	222.7	118.1	33.7	4.6	34.5	7.8
PBAT	-	117.1	-	10.2	-	8.9
Second heating						
PA6	222.3	-	71.8	-	31.2	-
PA6-20PBAT	221.5	-	62.4	-	34.3	-
PA6-30PBAT	221.2	118.6	52.1	1.7	33.3	4.7
PA6-40PBAT	222.1	117.7	41.2	2.5	30.9	5.2
PA6-50PBAT	221.1	116.3	35.2	4.1	31.9	6.9
PBAT	-	117.8	-	11.7	-	10.3

3.4. Mechanical Characterization

Figure 7a shows representative stress-strain curves from the tensile tests performed on the prepared blends, while Figure 7b–d reports the trends of elastic modulus (E), tensile strength (σ_{max}) and elongation at break (ϵ_b), compared also with the theoretical prediction of the ME model (see Equation (2)). Moreover, the results collected from the Vicat grade tests are shown in Figure 7e.

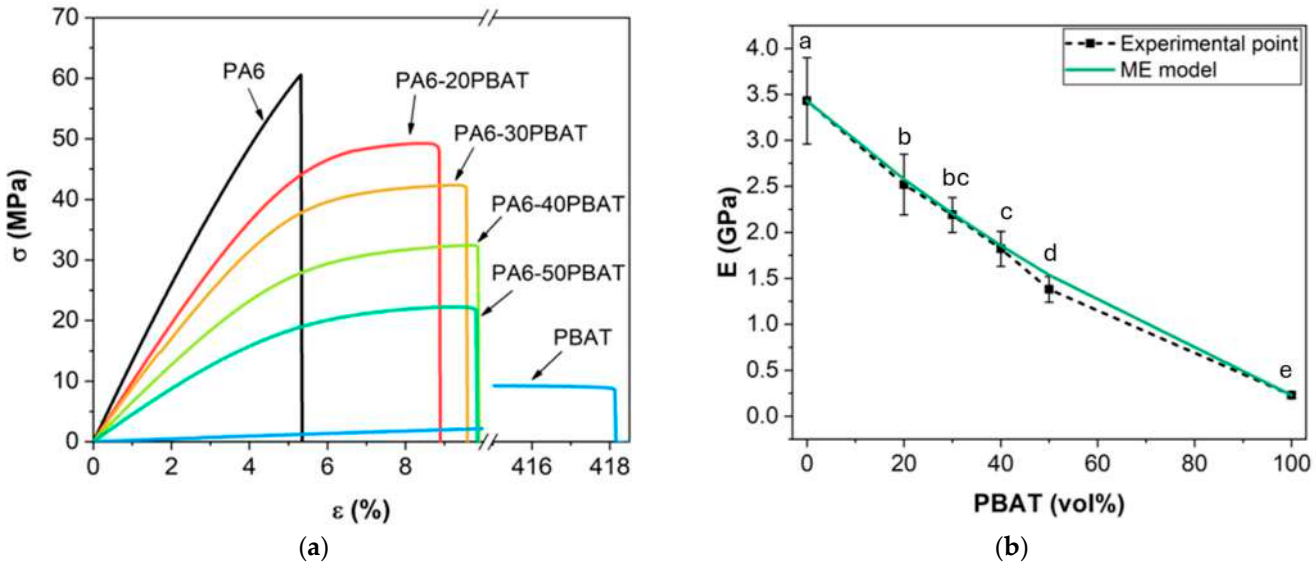

(**a**) (**b**)

Figure 7. *Cont.*

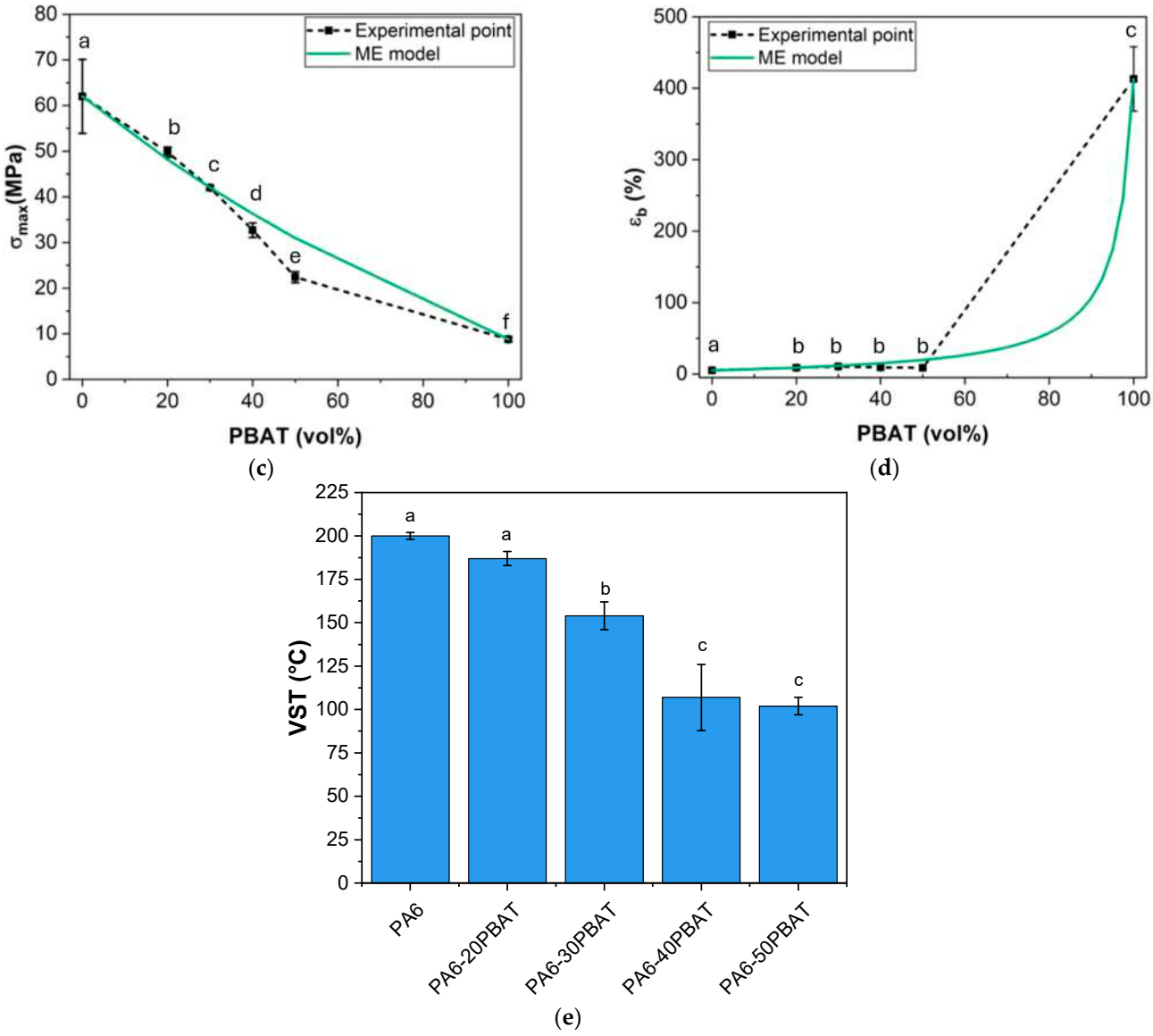

Figure 7. (**a**) Representative stress-strain curves from tensile tests performed on the prepared blends (the x-axis has been cut to reveal the property at break of PBAT). Trends of (**b**) elastic modulus (E), (**c**) tensile strength (σ_{max}) and (**d**) elongation at break (ϵ_b) as a function of PBAT volume content, in comparison with the ME model predictions. (**e**) Results form Vicat grade tests on the prepared blends. Different superscript letters indicate statistically significant differences between groups ($p < 0.05$).

Neat PA6 exhibits an elastic modulus of 3.4 GPa, a tensile strength of 62 MPa and an elongation at break of 5.2%, values that are in good agreement with those reported in the literature for this matrix [29,46]. In contrast, neat PBAT shows a much lower stiffness, with an elastic modulus of 0.2 GPa and a tensile strength of 9 MPa, while displaying a markedly higher ductility, as indicated by an elongation at break of 413%, also consistent with literature data [26]. As expected, the incorporation of PBAT into the PA6 matrix generally results in a reduction in both elastic modulus and tensile strength, reflecting the softer and ductile nature of the PBAT phase and also the immisciblility of these blends. For instance, the addition of 30%vol of PBAT leads to a decrease in modulus of approximately 36% and a σmax drop of about 32%, while the elongation at break increases by 102%. Notably, PA6-50PBAT formulation shows the stronger drop in mechanical performance, with a decreases of 60% in elastic modulus and 64% in tensile strength relative to neat PA6, without a further improvement in elongation at break. Generally, the experimental trends of mechanical properties

are in good agreement with the Maxwell–Eucken (ME) model for blends containing up to 40%vol PBAT. This indicates that the mechanical behavior of these formulations is well described by a droplet-like morphology with a continuous PA6 matrix and dispersed PBAT domains (observed in the SEM micrographs of Figure 5b–d). However, a clear deviation from the ME prediction is observed for the PA6–50PBAT blend, possibly due to the fact that phase inversion occured, as evidenced by the rheology and SEM micrograph in Figure 3a–c and Figure 5e, respectively. At this composition, the assumption of a continuous PA6 matrix is no longer valid, leading thus to a consequent mismatch between ME model predictions and experimental results. In view of the possible application of these blends as matrices for self-healing composite laminates, a PBAT content of 20–30%vol has been found to provide an acceptable drop of strength and stiffness (compared to neat PA6), while higher PBAT loadings result in a excessive reduction in both the modulus and the tensile strength values. Regarding Vicat grade values, PA6 exhibits the highest VST (i.e., 200 °C), indicating an optimal dimensional stability. However, it was not possible to acquire data for neat PBAT sample, as the needle penetrated too deeply into the sample due to its inherently lower Tm and stiffness. The VST follows a progressive decrease with the PBAT amount in the blends. For example, by introducing 30%vol of PBAT, the VST value is decresed to 154 °C and by introducing 50%vol of PBAT it further drops down to to 102 °C. Nevertheless, the VST values remain relatively high up to a PBAT content of 30%vol, highlighting that this formulation still retains suitable thermo-mechanical stability for being utilized as matrices in thermoplastic structural composites.

Based on these preliminary morphological and thermo-mechanical results, the PA6-30PBAT blend was selected for further evaluation of fracture toughness and self-healing capability. The results reported in Table 3 describe the fracture behaviour of neat PA6 and the PA6-30PBAT blend, tested both in quasi-static and impact mode, in terms of their K_{IC} and G_{IC} values.

Table 3. Critical stress intensity factor (K_{IC}) and critical strain energy release rate (G_{IC}) of neat PA6 and the PA6-30PBAT blend, measured in quasi-static and impact mode.

Samples	Quasi-Static Mode		Impact Mode
	K_{IC} ($MPa \cdot \sqrt{m}$)	G_{IC} (kJ/m^2)	K_{IC} ($MPa \cdot \sqrt{m}$)
PA6	3.58 ± 0.58 [a]	4.27 ± 1.13 [a]	3.08 ± 0.14 [a]
PA6-30PBAT	2.16 ± 0.09 [b]	3.21 ± 0.34 [a]	1.93 ± 0.15 [b]

Different superscript letters indicate statistically significant differences between groups ($p < 0.05$).

In quasi-static mode, neat PA6 exhibits a fracture toughness K_{IC} of 3.58 ± 0.58 $MPa \cdot \sqrt{m}$ and a critical strain energy release rate G_{IC} of 4.27 ± 1.13 kJ/m^2, in perfect agreement with the literature (i.e., approximately 2–4 $MPa \cdot \sqrt{m}$ for K_{IC} and 3–5 kJ/m^2 for G_{IC} [47]). The incorporation of PBAT results in a 39% reduction in K_{IC} compared to neat PA6. This decrease could be due to a rather weak interfacial adhesion between the two immiscible phases, which reduces the efficiency of stress transfer across the interface. Consequently, the load-bearing capability of the PA6 matrix is reduced during crack propagation. While no significant interfacial debonding was observed in the SEM micrographs (Figure 5c), the interface may not be sufficiently robust to effectively transfer stresses under fracture loading. In future work, the use of a suitable compatibilizer (different from the ones already tested during preliminary analyses, reported in Section 2.1) could be therefore considered. Similarly, G_{IC} decreases by approximately 25% upon PBAT incorporation, although these values are not statistically significant. The reduction in G_{IC} indicates lower resistance to crack initiation and propagation, which is likely again associated with the presence of

dispersed PBAT that does not properly adhere to the matrix, thus limiting the energy dissipation capability during fracture. Moreover, the inherently lower stiffness and tensile strength of PBAT compared to PA6 further contribute to this reduction. Under impact loading, the fracture toughness of neat PA6 is 3.08 MPa·√m, i.e., slightly lower than that measured in quasi-static mode. This reduction is attributed to the higher deformation rate that could have altered the viscoelastic response of the material, resulting in lower peak loads during testing. Such behaviour highlights that different mechanisms govern crack initiation and propagation under quasi-static and impact conditions [29]. The incorporation of PBAT leads to a statistically significant reduction in the impact K_{IC} value compared to neat PA6 (approximately 37%), similarly to quasi-static conditions. The findings are further supported by FESEM micrographs of the fracture surfaces of SENB specimens after testing, shown in Figure 8.

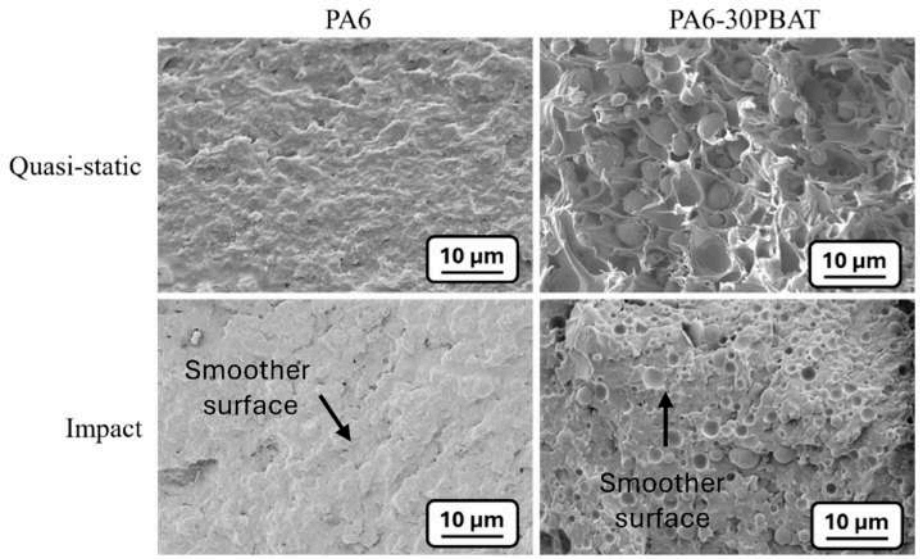

Figure 8. FESEM micrographs of the fracture surface of the SENB specimens tested in quasi-static and impact mode.

The fracture morphology differs markedly between the specimens tested in quasi-static and impact conditions. In quasi-static mode, both neat PA6 and the PA6-30PBAT blend display pronounced plastic deformation, with the fracture surface appearing particularly irregular. Conversely, specimens tested under impact conditions exhibit smoother fracture surfaces, with less evidence of plastic deformation in the neat PA6 and only limited deformation in PA6-30PBAT. As observed in previous works by our group [26,29,33], smoother crack surfaces facilitate the healing process by enabling the healing agent to spread more uniformly across the fracture plane, whereas rough and highly deformed surfaces hinder diffusion and wetting. For this reason, in this work impact testing mode was selected as the technique for the evaluation of the healing efficiency of the prepared blends.

3.5. Evaluation of Self-Healing Efficiency

Table 4 summarizes the fracture toughness values of the healed specimens ($K_{IC,H}$), alongside the corresponding self-healing efficiency (HE) values, measured under impact mode. The values referred to neat PA6 have not been reported, since it does not show any recovery of fracture toughness, regardless of the healing time and pressure applied.

The analysis of the fracture toughness values ($K_{IC,H}$) of the healed specimens demonstrates that the presence of PBAT is essential to achieve a partial fracture toughness recovery. At 1 MPa, by increasing the healing time from 30 to 120 min, the healing efficiency statisti-

cally increases from 16.1 ± 5.3% up to 28.0 ± 2.7%. At 2 MPa, the healing response remains nearly constant (~22%), indicating limited sensitivity to healing time. At 3 MPa, a slight improvement (but not statistically significant) can be observed at longer healing times, reaching 25.9 ± 6.5% after 120 min. However, the observed differences among healing conditions are not particularly pronounced, suggesting that neither pressure nor healing duration dramatically enhances fracture toughness recovery. Figure 9 shows the FESEM micrographs of the fracture surfaces of healed PA6-30PBAT specimens after healing performed at different times and pressures, to further corroborate these considerations.

Table 4. Critical stress intensity factor of healed PA6-30PBAT blend ($K_{IC,H}$) and its healing efficiency values (HE) as a function of healing pressure and time.

Sample	Pressure (MPa)	Time (min)	$K_{IC,H}$ (MPa·√m)	HE (%)
PA6-30PBAT	1	30	0.31 ± 0.10 [a]	16.1 ± 5.3 [a]
		60	0.38 ± 0.0 6 [a]	19.7 ± 3.5 [a]
		120	0.54 ± 0.03 [b]	28.0 ± 2.7 [b]
	2	30	0.42 ± 0.05 [a]	21.8 ± 3.1 [a]
		60	0.42 ± 0.05 [a]	21.8 ± 3.1 [a]
		120	0.43 ± 0.05 [a]	22.3 ± 3.1 [a]
	3	30	0.38 ± 0.16 [ab]	19.7 ± 8.4 [ab]
		60	0.42 ± 0.06 [a]	21.8 ± 3.5 [a]
		120	0.50 ± 0.12 [ab]	25.9 ± 6.5 [ab]

Different superscript letters indicate statistically significant differences between groups ($p < 0.05$).

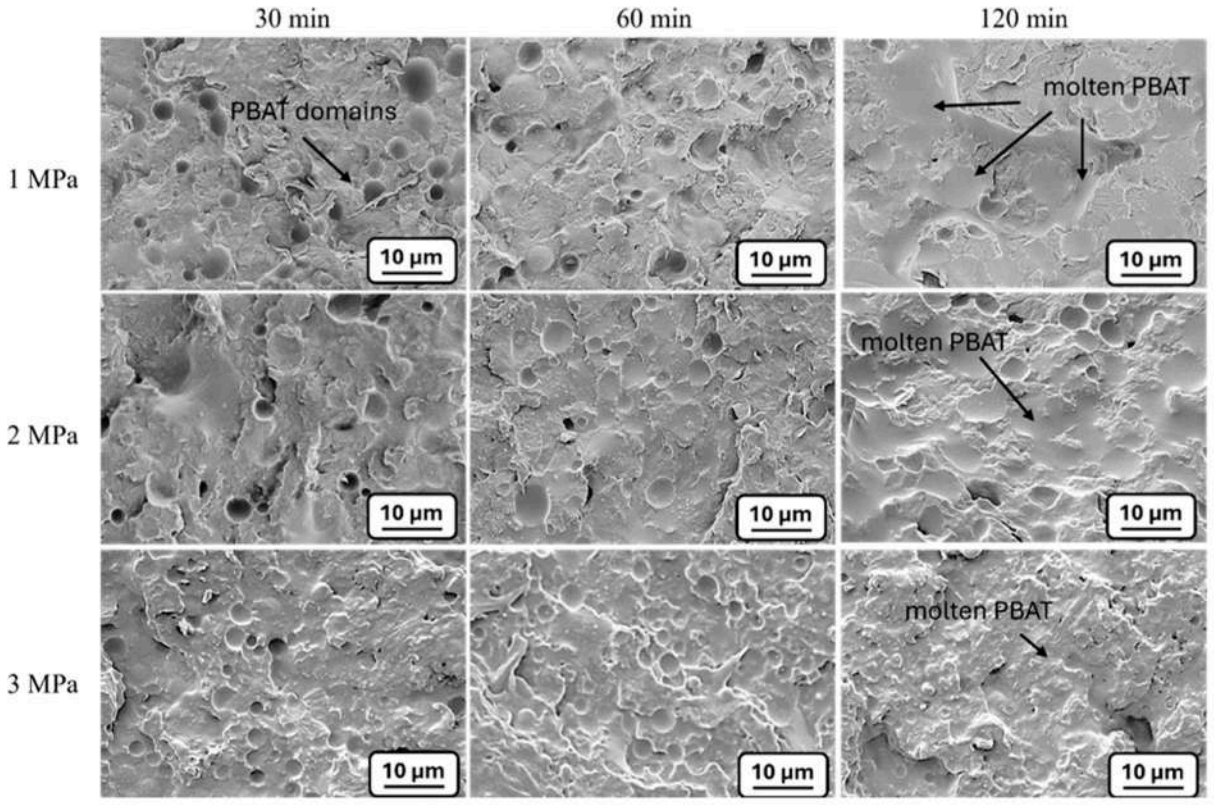

Figure 9. FESEM micrographs of the fracture surface of the healed PA6-30PBAT SENB specimens after testing in impact mode, as a function of healing time and pressure.

In principle, successful healing relies on the melting and flow of the dispersed PBAT phase within the PA6 crack plane. Consequently, effective repair should lead to the formation of a continuous PBAT interfacial film bridging the PA6 fractured surfaces, rather than retaining the original spherical domains [26]. At 1 MPa, the increase of the healing time from 30 to 120 min results in a noticeable change in the fracture surface, with less evidence of distinct PBAT domains. This morphological change is accompanied by the increase in healing efficiency observed in Table 4, suggesting that longer healing period allows PBAT to efficiently melt and flow across the interface, thus favoring the partial recovery of the fracture toughness. In contrast, increasing the pressure to 2 MPa produces fracture surfaces that remain relatively similar between them regardless of healing time, with the presence of discrete PBAT domains and limited evidence of the formation of a continuous interfacial film (only a few traces of molten PBAT are visible after 120 min). Consistently, the healing efficiency remains nearly constant. This behaviour suggests that the higher applied pressure may constrain the molten PBAT, limiting its ability to flow and spread within the crack plane. A further increase in pressure to 3 MPa appears to restrict material flow even more, resulting in no significant improvement in healing efficiency after 30 and 60 min. However, after 120 min, the fracture surface exhibits a more continuous PBAT film, accompanied by a slight increase in healing efficiency. This observation indicates that prolonged thermal exposure can partially compensate for the reduced phase mobility imposed by the higher pressure, by allowing sufficient time for the PBAT to melt and redistribute across the fracture interface. In future research, the influence of PBAT on the viscoelastic behaviour of the blend will be also investigated through dynamic mechanical analysis (DMA), in order to provide further insight on its role in the self-healing mechanism. Overall, the combined mechanical and microstructural observations indicate that healing performance is controlled by a balance between time to allow PBAT melting and diffusion and low pressure to avoid the constraining of the phase flow. Among the investigated conditions, 1 MPa for 120 min appears to provide the most favorable compromise for repairing the PA6–30PBAT blend, resulting in the highest healing efficiency (28%). In general, thermoplastic self-healing systems present in the literature have shown higher healing efficiencies. Specifically, Savioli et al. [26] obtained up to 64% in PLA/PBAT blends, Perin et al. [44] reached up to 35% in PA6/COC blends and Georgopoulou et al. [48] reached up to 68% in thermoplastic polyurethane (TPU)/ethylene vinyl acetate (EVA) blends. However, a direct quantitative comparison between the system investigated in this work and the others present in the literature should be made with caution because the polymer matrices, blend morphologies and healing mechanisms can substantially differ.

4. Conclusions

In this work, polyamide 6/poly(butylene adipate terephthalate) (PA6/PBAT) blends were developed by melt compounding and systematically characterized to assess their suitability as self-healing matrices for structural thermoplastic composites. Their rheological, morphological, thermal and mechanical properties were investigated, with particular emphasis on fracture toughness and thermal self-healing performance. Rheological analysis revealed a progressive decrease in the storage modulus (G′), loss modulus (G″) and complex viscosity (η) with increasing PBAT content, while maintaining melt processability compatible with conventional processing techniques. FESEM observations confirmed the formation of an immiscible blend morphology, consisting of uniformly dispersed PBAT domains within the continuous PA6 matrix, with rather good interfacial adhesion between the two phases. From a mechanical point of view, increasing the content of PBAT resulted in a significant reduction in stiffness and strength. However, the addition of 30%vol of PBAT was found to provide acceptable tensile properties and Vicat grade compared to neat PA6.

The evaluation of fracture toughness under quasi-static and impact conditions revealed that introducing PBAT at a concentration of 30%vol slightly decreased the K_{IC} value by about 39% in quasi-static mode and 37% in impact conditions. This could be attributed to weak interfacial adhesion between the two materials and the inherently lower stiffness and strength of PBAT. Self-healing capability was assessed by measuring the recovery of fracture toughness in SENB samples after they were heated to 150 °C. While neat PA6 showed no healing, a partial repair was observed for the blend containing 30%vol of PBAT. The effects of healing time (30 to 120 min) and pressure (1 to 3 MPa) on the repair efficiency of this blend were investigated. Even if the change of these parameters had a limited influence on the healing performance, the best results were obtained at 1 MPa for 120 min with a healing efficiency value of 28%, while the prolonged thermal exposure allowed the PBAT dispersed phase to sufficiently reduce its viscosity, melt, and flow across the crack interface, forming a more homogeneous interfacial layer and maximizing fracture toughness recovery. Since the formulation with 30%vol of PBAT represented the best balance between mechanical performance and self-healing efficiency, it could be investigated in the future for the preparation of multifunctional composite laminates with self-healing capability.

Supplementary Materials: The following supporting information can be downloaded at: https://www.mdpi.com/article/10.3390/jcs10080435/s1, Figure S1: Dynamic rheological behaviour of the uncompatibilized and compatibilized blends (T = 230 °C). Trends of (a) storage modulus, (b) loss modulus and (c) complex viscosity as a function of the angular frequency. The compatibilized blend is listed as PA6-30PBAT-J; Figure S2: Representative stress-strain curves from tensile tests performed on the uncompatibilized and compatibilized blends; Table S1: Values of tensile modulus, strength and elongation at break of the uncompatibilized and compatibilized blends; Figure S3: Values of fracture toughness of the uncompatibilized and compatibilized blends before (K_{IC}) and after ($K_{IC,H}$) healing.

Author Contributions: Conceptualization, L.S., A.S. and A.D.; methodology, L.S., A.S. and A.D.; validation, L.S., A.S., A.P. and A.D.; formal analysis, L.S., G.F. and A.S.; investigation, L.S., G.F. and A.S.; resources, A.D.; data curation, L.S. and G.F.; writing—original draft preparation, L.S.; writing—review and editing, A.S., A.P. and A.D.; visualization, L.S., A.S., A.P. and A.D.; supervision, A.D.; project administration, L.S., A.S. and A.D.; funding acquisition, A.D. All authors have read and agreed to the published version of the manuscript.

Funding: This research received no external funding.

Institutional Review Board Statement: Not applicable.

Informed Consent Statement: Not applicable.

Data Availability Statement: The raw data supporting the conclusions of this article will be made available by the authors on request.

Conflicts of Interest: The authors declare no conflicts of interest.

References

1. Koniuszewska, A.; Kaczmar, J. Application of polymer based composite materials in transportation. *Prog. Rubber Plast. Recycl. Technol.* **2016**, *32*, 1–24. [CrossRef]
2. Bas, O.; Ates, E.; Ozturk, F. Thermoplastic Composite Materials for the Aerospace Industry. *Res. Dev. Mater. Sci.* **2021**, *15*, 1745–1748. [CrossRef]
3. Luo, Y.; Lin, G.; Chen, J.F.; Wu, J. Thermoplastic fiber-reinforced polymer composites in construction: A state-of-the-art review. *Case Stud. Constr. Mater.* **2025**, *23*, 5596–5624. [CrossRef]
4. Truschelli, N.; Simonini, L.; Tempelis, A.; Mishnaevsky, L., Jr.; Pegoretti, A.; Dorigato, A. Development of self-healing epoxy/COC adhesives for potential use in wind turbine blades. *Compos. Part A Appl. Sci. Manuf.* **2026**, *205*, 109732–109744. [CrossRef]
5. GrandViewResearch. Thermoplastic Composites Market (2022–2030). 2021. Available online: https://www.grandviewresearch.com/industry-analysis/thermoplastic-composites-market-report (accessed on 13 April 2026).

6. Silu, H.; Bo, W.; Libo, Y. Interphase and Interfacial Properties of Composite Materials. In *Composite Materials: Manufacturing, Properties and Applications*; Low, I.M., Dong, Y., Eds.; Elsevier: Amsterdam, The Netherlands, 2021; pp. 151–177.
7. Romanowic, P.; Muc, A. Estimation of Notched Composite Plates Fatigue Life Using Residual Strength Model Calibrated by Step-Wise Tests. *Materials* **2018**, *11*, 2180. [CrossRef] [PubMed]
8. Simonini, L.; Mahmood, H.; Dorigato, A.; Alessandro, P. Development of a self-healing interphases for structural composites. In Proceedings of the 23rd International Conference on Composite Materials, ICCM 2023, Belfast, UK, 30 July–4 August 2023.
9. Mahmood, H.; Simonini, L.; Dorigato, A.; Pegoretti, A. Graphene Deposition on Glass Fibers by Triboelectrification. *Appl. Sci.* **2021**, *11*, 3123. [CrossRef]
10. Simonini, L.; Mahmood, H.; Dorigato, A.; Pegoretti, A. Evaluation of self-healing capability of a polycaprolactone interphase in epoxy/glass composites. *Compos. Part A Appl. Sci. Manuf.* **2023**, *169*, 107539–107548. [CrossRef]
11. Simonini, L.; Kakkonen, M.; Dsouza, R.; Kanerva, M.; Mahmood, H.; Dorigato, A.; Pegoretti, A. Tailoring the interfacial properties of glass fiber-epoxy microcomposites through the development of a self-healing poly (ϵ-caprolactone) coating. *Compos. Sci. Technol.* **2025**, *261*, 110991–111007. [CrossRef]
12. Sun, Y.; Simonini, L.; Xing, C.; Mishnaevsky, L., Jr. Self-healing interfaces in fiber reinforced polymers: Computational modeling. *Compos. Sci. Technol.* **2025**, *270*, 111269–111282. [CrossRef]
13. Simonini, L.; Canale, R.; Mahmood, H.; Dorigato, A.; Pegoretti, A. Multifunctional epoxy/carbon composites with a fully reparable interface. *Polym. Compos.* **2024**, *45*, 2558–2568. [CrossRef]
14. Simonini, L.; Dorigato, A. Surface Modification of Wood Fibers with Citric Acid as a Sustainable Approach to Developing Novel Polycaprolactone-Based Composites for Packaging Applications. *J. Compos. Sci.* **2025**, *9*, 274. [CrossRef]
15. Mahmood, H.; Dorigato, A.; Pegoretti, A. Healable Carbon Fiber-Reinforced Epoxy/Cyclic Olefin Copolymer Composites. *Materials* **2020**, *13*, 2165. [CrossRef] [PubMed]
16. Zovi, R.C.; Mahmood, H.; Dorigato, A.; Fredi, G.; Pegoretti, A. Cyclic Olefin Copolymer Interleaves for Thermally Mendable Carbon/Epoxy Laminates. *Molecules* **2020**, *25*, 5347. [CrossRef] [PubMed]
17. Cohades, A.; Branfoot, C.; Rae, S.; Bond, I.; Michaud, V. Progress in Self-Healing Fiber-Reinforced Polymer Composites. *Adv. Mater. Interfaces* **2018**, *5*, 1800177. [CrossRef]
18. Trask, R.S.; Williams, H.R.; Bond, I.P. Self-healing polymer composites: Mimicking nature to enhance performance. *Bioinspir. Biomim.* **2007**, *2*, P1. [CrossRef] [PubMed]
19. Jones, A.R.; Blaiszik, B.J.; White, S.R.; Sottos, N.R. Full recovery of fiber/matrix interfacial bond strength using a microencapsulated solvent-based healing system. *Compos. Sci. Technol.* **2013**, *79*, 1–7. [CrossRef]
20. Norris, C.J.; Meadway, G.J.; O'Sullivan, M.J.; Bond, I.P.; Trask, R.S. Self-healing fibre reinforced composites via a bioinspired vasculature. *Adv. Funct. Mater.* **2011**, *21*, 3624–3633. [CrossRef]
21. Ghazali, H.; Ye, L.; Amir, A.N. Microencapsulated healing agents for an elevated-temperature cured epoxy: Influence of viscosity on healing efficiency. *Polym. Polym. Compos.* **2021**, *29*, 1317–1327. [CrossRef]
22. Zhang, W.; Duchet, J.; Gerard, J.F. Self-healable interfaces based on thermo-reversible Diels–Alder reactions in carbon fiber reinforced composites. *J. Colloid Interface Sci.* **2014**, *430*, 61–68. [CrossRef] [PubMed]
23. Zhang, H.; Lamnawar, K.; Maazouz, A. Rheological modeling of the diffusion process and the interphase of symmetrical bilayers based on PVDF and PMMA with varying molecular weights. *Rheol. Acta* **2012**, *51*, 691–711. [CrossRef]
24. Wu, D.Y.; Sam Meure, S.; Solomon, D. Self-healing polymeric materials: A review of recent developments. *Prog. Polym. Sci.* **2008**, *33*, 479–522. [CrossRef]
25. Islam, S.; Bhat, G. Progress and challenges in self-healing composite materials. *Mater. Adv.* **2012**, *2*, 1896–1926.
26. Savioli, I.; Simonini, L.; Rigotti, D.; Pegoretti, A.; Dorigato, A. Biodegradable Poly (lactic acid)-Based Blends as Intrinsic Self-Healing Matrices for Multifunctional and Eco-Sustainable Composites. *Molecules* **2026**, *31*, 921. [CrossRef] [PubMed]
27. Peñas-Caballero, M.; Santana, M.H.; Verdejo, R.; Lopez-Manchado, M.A. Polymer blends as an effective strategy to designing self-healing epoxy resin. *Compos. Part A Appl. Sci. Manuf.* **2025**, *200*, 109390–109402. [CrossRef]
28. Kohutiar, M.; Kakošová, L.; Krbata, M.; Janík, R.; Fekiač, J.J.; Breznická, A.; Timárová, L. Comprehensive review: Technological approaches, properties, and applications of pure and reinforced polyamide 6 (PA6) and polyamide 12 (PA12) composite materials. *Polymers* **2025**, *17*, 442. [CrossRef] [PubMed]
29. Perin, D.; Odorizzi, G.; Dorigato, A.; Pegoretti, A. Development of polyamide 6 (PA6)/polycaprolactone (PCL) thermoplastic self-healing polymer blends for multifunctional structural composites. *Appl. Sci.* **2022**, *12*, 12357. [CrossRef]
30. Frontechnic. What Does PA6 Stand For? Polyamide 6 Explained. 2026. Available online: https://www.frontechnic.com/news/industry-news/what-does-pa6-stand-for-polyamide-6-explained.html (accessed on 27 April 2026).
31. Wang, P.; Yang, L.; Zhou, Y.; Gao, S.; Cao, T.; Feng, S.; Xu, P.; Ding, Y. Synergistic effect of EVA-GMA and nanofillers on mechanical and dielectric properties of polyamide. *Compos. Commun.* **2021**, *25*, 100738–100743. [CrossRef]
32. Kondo, M.Y.; Montagna, L.S.; Morgado, G.F.D.M.; Castilho, A.L.G.D.; Batista, L.A.P.D.S.; Botelho, E.C.; Ribeiro, M.V. Recent advances in the use of Polyamide-based materials for the automotive industry. *Polímeros* **2022**, *32*, 2022023–2022036. [CrossRef]

33. Perin, D.; Dorigato, A.; Pegoretti, A. Compatibilization of polyamide 6/cyclic olefinic copolymer blends for the development of multifunctional thermoplastic composites with self-healing capability. *Materials* **2024**, *17*, 1880. [CrossRef] [PubMed]
34. Perin, D.; Botta, L.; Rigotti, D.; Dorigato, D.; Fredi, G.; Pegoretti, A. Tuning the compatibilizer content and healing temperature in thermally mendable polyamide 6/cyclic olefinic copolymer blends. *Polymers* **2025**, *17*, 280. [CrossRef] [PubMed]
35. Diao, X.; Zhang, C.; Weng, Y. Properties and degradability of poly (butylene adipate-co-terephthalate)/calcium carbonate films modified by polyethylene glycol. *Polymers* **2022**, *14*, 484. [CrossRef] [PubMed]
36. Millot, C.; Fillot, L.A.; Lame, O.; Sotta, P.; Seguela, R. Assessment of polyamide-6 crystallinity by DSC: Temperature dependence of the melting enthalpy. *J. Therm. Anal. Calorim.* **2015**, *122*, 307–314.
37. Wang, J.F.; Carson, J.K.; North, M.F.; Cleland, D.J. A knotted and interconnected skeleton structural model for predicting Young's modulus of binary phase polymer blends. *Polym. Eng. Sci.* **2010**, *50*, 643–651. [CrossRef]
38. Yıldırım, R.; Mert, O.; Ozkoc, G.; Kodal, M. Enhanced recyclability of thermoplastic elastomer toughened polyamide 6 via tri-and multi-epoxy-terminated POSS hybrid additives. *ACS Omega* **2024**, *9*, 45467–45486. [CrossRef] [PubMed]
39. Kherroub, D.E.; Belbachir, M.; Lamouri, S.; Bouhadjar, L.; Chikh, K. Synthesis of polyamide-6/montmorillonite nanocomposites by direct in-situ polymerization catalysed by exchanged clay. *Orient. J. Chem.* **2013**, *29*, 1429–1436. [CrossRef]
40. Lim, M.-Y.; Kim, H.J.; Baek, S.J.; Kim, K.Y.; Lee, S.S.; Lee, J.C. Improved strength and toughness of polyketone composites using extremely small amount of polyamide 6 grafted graphene oxides. *Carbon* **2014**, *77*, 366–378. [CrossRef]
41. De Campos Vidal, B. Using the FT-IR linear dichroism method for molecular order determination of tendon collagen bundles and nylon 6. *Acta Histochem.* **2013**, *115*, 686–691. [CrossRef] [PubMed]
42. Zhang, X.; Bian, H.; Meng, X.; Yuan, J.; Ding, J.; Li, W.; Guo, B. Synthesis of Poly (butylene adipate-co-terephthalate) with Branched Monomer for Biodegradable Copolyesters with Enhanced Processability and Rheological Properties. *ACS Omega* **2025**, *10*, 14258–14270. [CrossRef] [PubMed]
43. Kanwal, A.; Zhang, M.; Sharaf, F.; Li, C. Enzymatic degradation of poly (butylene adipate co-terephthalate)(PBAT) copolymer using lipase B from *Candida antarctica* (CALB) and effect of PBAT on plant growth. *Polym. Bull.* **2022**, *79*, 9059–9073. [CrossRef]
44. Perin, D.; Dorigato, A.; Pegoretti, A. Thermoplastic self-healing polymer blends for structural composites: Development of polyamide 6 and cyclic olefinic copolymer blends. *J. Appl. Polym. Sci.* **2023**, *140*, 53751–53768. [CrossRef]
45. Xiao, H.; Lu, W.; Yeh, J.T. Crystallization behavior of fully biodegradable poly (lactic acid)/poly (butylene adipate-co-terephthalate) blends. *J. Appl. Polym. Sci.* **2009**, *112*, 3754–3763. [CrossRef]
46. Amroune, S.; Saib, C.; Houari, A.; Zergane, S.; Mohamad, B.A.; Madani, K.; Aichouche, M.L.; Zidane, M. Analysis and manufacturing of truck trailer supports in polyamide PA6. *Int. J. Struct. Integr.* **2025**, *16*, 384–402. [CrossRef]
47. Siengchin, S.; Karger-Kocsis, J. Structure, mechanical, and fracture properties of nanoreinforced and HNBR-toughened polyamide-6. *J. Appl. Polym. Sci.* **2012**, *123*, 897–902. [CrossRef]
48. Georgopoulou, A.; Klein, J.; Eckey, L.M.; Susoff, M.; Clemens, F. Self-healing thermoplastic elastomer blends with hybrid fillers for piezoresistive and humidity sensing applications. *Chem. Eng. J.* **2025**, *526*, 170993–171002. [CrossRef]